Atomic Structure of Steps on 180° Ferroelectric Domain Walls in $PbTiO_3$*

Arzhang Angoshtari and Arash Yavari†
School of Civil and Environmental Engineering, Georgia Institute of Technology, Atlanta, GA 30332.
(Dated: September 20, 2010)

Using the method of anharmonic lattice statics, we calculate the equilibrium structure of steps on 180° ferroelectric domain walls (DW) in $PbTiO_3$. We consider three different types of steps: i) Ti-Ti step that joins a Ti-centered DW to a Ti-centered DW, (ii) Pb-Pb step that joins a Pb-centered DW to a Pb-centered DW, and (iii) Pb-Ti step that joins a Pb-centered DW to a Ti-centered DW. We show that atomic distortions due to these steps broaden a DW but are localized, i.e., they are confined to regions with dimensions of a few lattice spacings. We see that a step locally thickens the domain wall; the defective domain wall is two to three times thicker than the perfect domain wall depending on the step type. We also observe that steps distort the polarization distribution in a mixed Bloch-Néel like way; polarization rotates out of the domain wall plane near the steps. Our calculations show that Pb-Pb steps have the lowest static energy.

I. INTRODUCTION

Ferroelectric materials are an important subclass of polar materials due to their wide range of applications in ultrasound imaging, microelectromechanical systems, high strain actuators, electro-optical systems, photothermal imaging, and high density storage devices [1]. It is known that some important properties of ferroelectric materials are due to the presence of domain walls, which are two-dimensional defects that separate regions with uniform polarization [2]. This explains the importance of a detailed study of the properties of the domain walls.

From both experimental and theoretical studies, it is observed that the thickness of domain walls can vary from a few angstroms [3–7] to a few micrometers [8, 9]. It has been suggested that this wide scatter in the domain wall thickness is due to the presence of point defects [10–12]. Another important property of domain walls is the behavior of the polarization profile near the domain wall. It is well known that 180° domain walls have an Ising-like nature. Using Monte-Carlo simulation, Padilla *et al.* [4] showed the predominant Ising-like character of 180° domain walls in tetragonal $BaTiO_3$ along the tetragonal axis. In 180° domain walls, polarization vector can either rotate in a plane parallel to the domain wall (Bloch type) or normal to the domain wall (Néel type) [13]. Subsequent works on the domain walls showed that domain walls can have mixed characters. Using density functional theory, Lee *et al.* [13] showed that while 180° domain walls in $PbTiO_3$ are predominantly Ising-like, they have some Néel characters as well. Having the domain walls parallel to the (100)-plane, we know that polarization is mainly along the $\langle 010\rangle$-direction (see Fig. 1). As Lee *et al.* [13] showed close to the domain wall polarization has normal components (normal to the domain wall) with magnitudes in the order of 1-2 percent of the bulk polarization. Angoshtari and Yavari [6] observed a similar behavior at finite temperatures for perfect 180° domain walls. They saw normal components in the order of 2 percent of the bulk polarization in their finite-temperature structure calculations. Recently, first-principle-based simulations have led to the prediction of vortex type polarization distribution in zero-dimensional ferroelectric nanodots [14, 15].

It is believed that steps have an important role in domain wall motion. Nettleton [16] proposed a model for sidewise displacement of a 180° domain wall in a single crystal barium titanate and suggested that the formation of an irregular pattern of steps of varying shapes and sizes results in the motion of the domain wall and the speed of the domain wall motion is determined by the rate of formation and disappearance of these steps. Shur *et al.* [17] considered steps on 180° domain walls and proposed a mechanism for domain wall motion in weak and strong fields. Shin *et al.* [18] used atomistic molecular dynamics and coarse-grained Monte Carlo simulations to analyze the nucleation and growth mechanism of domain walls in $PbTiO_3$ and $BaTiO_3$.

In this work we investigate the effect of steps, which are one-dimensional defects, on 180° domain walls parallel to (100)-planes in $PbTiO_3$ using the anharmonic lattice statics method. We consider Ti-Ti steps that join a Ti-centered DW to another Ti-centered DW, Pb-Pb steps that join a Pb-centered DW to another Pb-centered DW, and Pb-Ti steps that join a Pb-centered DW to a Ti-centered DW. As the initial configuration, we start from the atomic configuration of perfect 180° domain walls and then relax the structure iteratively to obtain the optimized atomic configuration.

This paper is organized as follows. In §II, we explain the initial geometry of steps that we analyzed throughout this work. In §III, we discuss the method of anharmonic lattice statics and the shell potential for $PbTiO_3$ that we used in our calculations. We present our numerical results in §IV. The paper ends with concluding remarks in §V.

*To appear in *Journal of Applied Physics*.
†Electronic address: arash.yavari@ce.gatech.edu

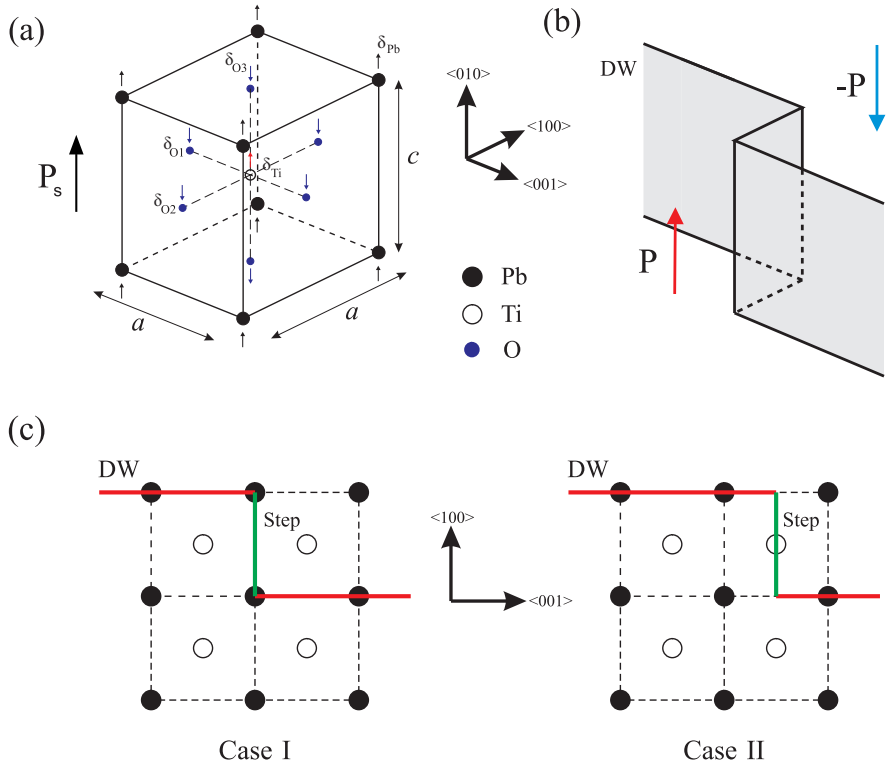

FIG. 1: (a) The relaxed configuration of the unit cell of tetragonal $PbTiO_3$. a and c are the tetragonal lattice parameters. Note that O1, O2, and O3 refer to oxygen atoms located on (001), (100), and (010)-planes, respectively. δ denotes the y-displacements of the atoms from the centerosymmetric position and arrows near each atom denote the direction of these displacements. (b) Schematic profile of polarization close to a step. (c) Two different possibilities for a Pb-Pb step.

II. GEOMETRY OF STEPS

The geometry of the relaxed unit cell of tetragonal $PbTiO_3$ is shown in Fig.1(a). The nonzero relative displacements in the $\langle 010 \rangle$-direction between the center of the positive and negative charges generate a polarization in the $\langle 010 \rangle$-direction (we are using a shell potential). In the 180° domain walls, direction of polarization switches across the domain wall. There are two types of 180° domain wall in $PbTiO_3$, namely, Ti-centered and Pb-centered domain walls. Using the relaxed bulk configurations, it is possible to calculate the atomic structure of both types [5].

Consider a domain wall parallel to a (100)-plane. By a step on the domain wall we mean the region where the domain wall joins another domain wall parallel to the first wall with an offset in the $\langle 100 \rangle$-direction (see Figs.1(b) and (c)).[25] We consider three different steps: Ti-Ti, Pb-Pb, and Pb-Ti. Fig.2 shows the unrelaxed initial configuration for each step. Note that assuming that the step is limited to a single unit cell, i.e. if the two domain walls are one or half a lattice spacing apart, there would be more than one possibility for the step configuration. As an example, we plot two possibilities for Pb-Pb step in Fig. 1(c). In this figure, Case I shows a Pb-Pb step in (001) PbO-plane while Case II shows another Pb-Pb step in (001) TiO_2-plane. Note that there are still other possibilities for Pb-Pb steps. We should emphasize that the configurations shown in Fig. 1(c) and Fig.2 are only the initial configurations that we use as the starting point for finding the final equilibrium configuration. We observe that as far as we confine the step to a single unit cell, the anharmonic lattice statics iterations converge to the same solution regardless of the initial configuration of the step. Therefore, the exact choice of the initial step configuration is not important in the final equilibrium structure. We should also emphasize that we are analyzing a single step on a single domain wall in an infinite crystal, i.e. no periodicity assumptions are made. Note that in Fig.2, domain walls away from the step have polarization only along the $\langle 010 \rangle$-direction. Note also that we assume a 2-D symmetry reduction, which means that all the atoms with the same x and z coordinates (x, y, and z are coordinates along the $\langle 100 \rangle$, $\langle 010 \rangle$, and $\langle 001 \rangle$-directions, respectively) have the same displacements. Therefore, we partition the 3-D lattice $\mathcal{L}$ as $\mathcal{L} = \bigsqcup_I \bigsqcup_{\alpha,\beta \in \mathbb{Z}} \mathcal{L}_{I\alpha\beta}$, where $\mathcal{L}_{I\alpha\beta}$ and $\mathbb{Z}$ are 1-D equivalence classes parallel to the $\langle 010 \rangle$-direction and the set of integers, respectively. See [19, 20] for more details on the symmetry reduction.

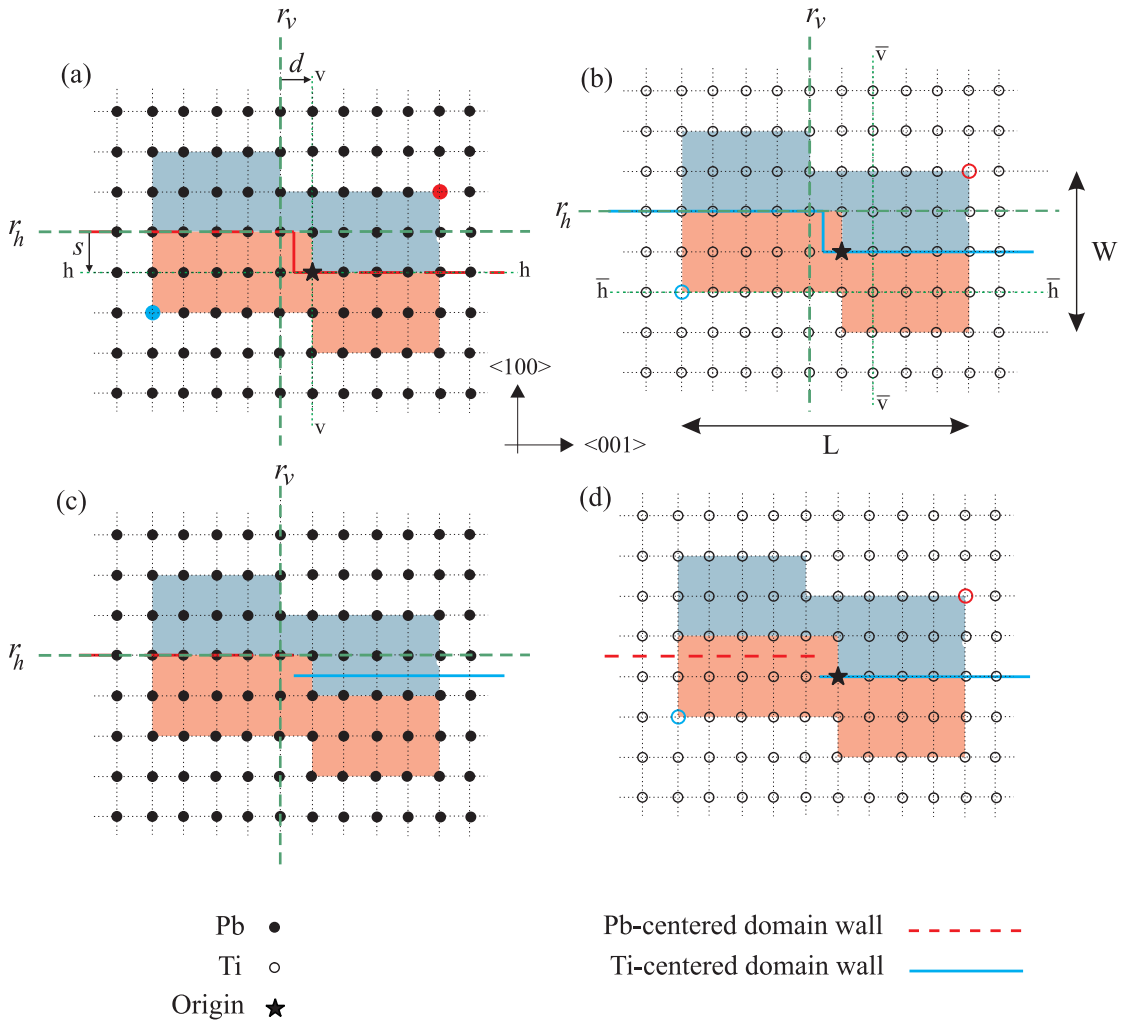

FIG. 2: A representative atomic layer for the initial configuration of the three steps: (a) Pb cores in Pb-Pb step, (b) Ti cores in Ti-Ti step, (c) Pb cores in Pb-Ti step, and (d) Ti cores in Pb-Ti step. Note that planes h-h and v-v are sections that are used for a better display of the variation of the distortion field in our numerical examples. s and d denote the distances of sections h-h and v-v from the reference planes r_h and r_v, respectively. r_h and r_v are parallel to (100) and (001)-planes, respectively. h-h and v-v sections in part (a) correspond to $s = a$ and $d = a$ and $\bar{\text{h}}$-$\bar{\text{h}}$ and $\bar{\text{v}}$-$\bar{\text{v}}$ sections in part (b) correspond to $s = 2a$ and $d = 2a$. The shaded regions denote the computational box, which contains $W \times L$ unit cells and different colors show the regions with opposite polarization inside the computational box. The symbol ★ in these figures denote the origin of the coordinate system in each type of steps. The blue and red filled and hollow circles denote the atoms whose displacements are used as the displacements of the atoms located outside of the computational box.

III. METHOD OF CALCULATION

We use the method of anharmonic lattice statics [19] to calculate the atomic structure of steps. We use a shell potential for $PbTiO_3$ [21] to model the atomic interactions. In this potential, each ion is represented by a core and a massless shell. Let $\mathcal{L}$ denote the collection of cores and shells, $i \in \mathcal{L}$ denote a core or a shell in $\mathcal{L}$, and $\{\mathbf{x}^i\}_{i\in\mathcal{L}}$ represent the current position of cores and shells. Then, the total static energy can be written as

$$\mathcal{E}\left(\{\mathbf{x}^i\}_{i\in\mathcal{L}}\right) = \mathcal{E}_{\text{short}}\left(\{\mathbf{x}^i\}_{i\in\mathcal{L}}\right) + \mathcal{E}_{\text{long}}\left(\{\mathbf{x}^i\}_{i\in\mathcal{L}}\right) + \mathcal{E}_{\text{core-shell}}\left(\{\mathbf{x}^i\}_{i\in\mathcal{L}}\right). \quad (1)$$

$\mathcal{E}_{\text{short}}\left(\{\mathbf{x}^i\}_{i\in\mathcal{L}}\right)$ denotes short range interactions, which are assumed to be only between Pb-O, Ti-O, and O-O shells. The short range interactions are described by the Rydberg potential of the form $(A + Br)\exp(-r/C)$, where A, B and C are potential parameters and r is the distance between interacting elements. $\mathcal{E}_{\text{long}}\left(\{\mathbf{x}^i\}_{i\in\mathcal{L}}\right)$ denotes the Coulombic interactions between the core and shell of each ion with the cores and shells of all of the other ions. Note that for calculating the classical Coulombic potential and force, we use the damped Wolf method [23]. Finally, $\mathcal{E}_{\text{core-shell}}\left(\{\mathbf{x}^i\}_{i\in\mathcal{L}}\right)$ represents the interaction of core and shell of an atom and

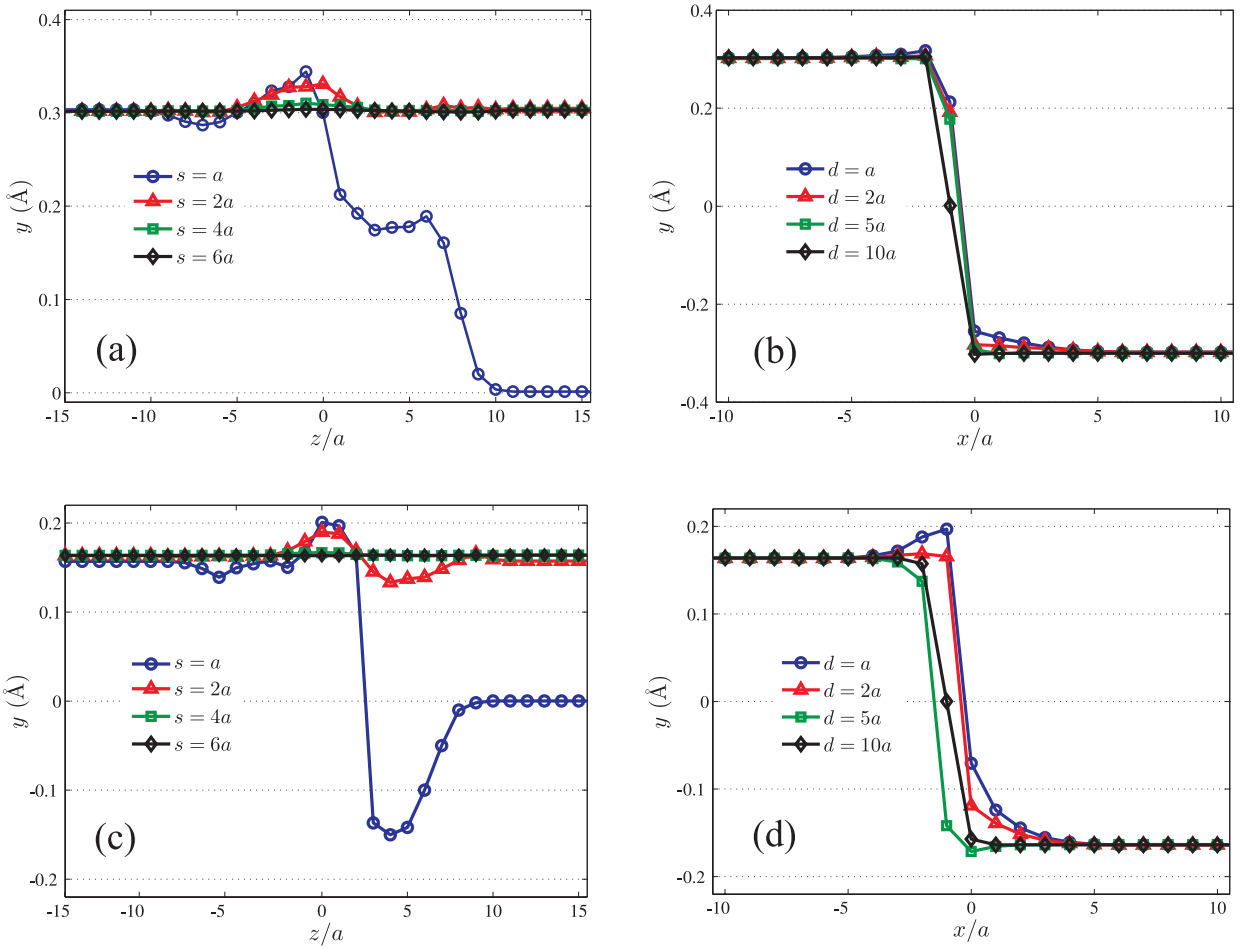

FIG. 3: The y-coordinates of atoms. (a) and (b) are Pb cores in a Pb-Pb step, (c) and (d) are Ti cores in a Ti-Ti step. Note that as it is shown in Fig.2, s and d denote the distances from the reference planes.

is assumed to be an anharmonic spring of the form $(1/2)k_2r^2 + (1/24)k_4r^4$, where k_2 and k_4 are constants. All calculations are done for absolute zero temperature. As is shown in Fig.1, at this temperature $PbTiO_3$ has a tetragonal unit cell with lattice parameters $a = 3.843$ Å and $c = 1.08a$ [21]. For more details on this notation see [20].

For the relaxed configuration $\mathcal{B} = \{\mathbf{x}^i\}_{i\in\mathcal{L}} \subset \mathbb{R}^3$, static energy attains a local minimum and hence we have

$$\frac{\partial \mathcal{E}}{\partial \mathbf{x}^i} = \mathbf{0} \qquad \forall\, i \in \mathcal{L}. \tag{2}$$

To obtain the solution of the above optimization problem we use the Newton method, which is based on a quadratic approximation near the current configuration $\mathcal{B}^k$:

$$\begin{aligned}\mathcal{E}\left(\mathcal{B}^k + \tilde{\boldsymbol{\delta}}^k\right) &= \mathcal{E}\left(\mathcal{B}^k\right) + \boldsymbol{\nabla}\mathcal{E}\left(\mathcal{B}^k\right)\cdot\tilde{\boldsymbol{\delta}}^k \\ &+ \frac{1}{2}(\tilde{\boldsymbol{\delta}}^k)^{\mathsf{T}}\cdot\mathbf{H}\left(\mathcal{B}^k\right)\cdot\tilde{\boldsymbol{\delta}}^k + o\left(|\tilde{\boldsymbol{\delta}}^k|^2\right),\end{aligned} \tag{3}$$

where $\tilde{\boldsymbol{\delta}}^k = \mathcal{B}^{k+1} - \mathcal{B}^k$ and $\mathbf{H}$ is the Hessian matrix. In the Newton method:

$$\tilde{\delta}^k = -\mathbf{H}^{-1}\left(\mathcal{B}^k\right)\cdot\boldsymbol{\nabla}\mathcal{E}\left(\mathcal{B}^k\right). \tag{4}$$

Having $\tilde{\boldsymbol{\delta}}^k$, the next configuration is calculated as: $\mathcal{B}^{k+1} = \mathcal{B}^k + \tilde{\boldsymbol{\delta}}^k$.

As the size of the simulation box increases, the calculation of the Hessian becomes inefficient and hence we use the quasi-Newton method. In this method, instead of calculating the Hessian in each iteration, one uses the Broyden-Fletcher-Goldfarb-Shanno (BFGS) algorithm to approximate the inverse of the Hessian [24]. One starts with a positive-definite matrix and uses the following BFGS algorithm to update the Hessian at each iteration:

$$\begin{aligned}\mathbf{C}^{i+1} &= \mathbf{C}^i + \frac{\tilde{\boldsymbol{\delta}}^k \otimes \tilde{\boldsymbol{\delta}}^k}{(\tilde{\boldsymbol{\delta}}^k)^{\mathsf{T}}\cdot\boldsymbol{\Delta}} - \frac{\left(\mathbf{C}^i\cdot\boldsymbol{\Delta}\right)\otimes\left(\mathbf{C}^i\cdot\boldsymbol{\Delta}\right)}{\boldsymbol{\Delta}^{\mathsf{T}}\cdot\mathbf{C}^i\cdot\boldsymbol{\Delta}} \\ &+ \left(\boldsymbol{\Delta}^{\mathsf{T}}\cdot\mathbf{C}^i\cdot\boldsymbol{\Delta}\right)\mathbf{u}\otimes\mathbf{u},\end{aligned} \tag{5}$$

where $\mathbf{C}^i = \left(\mathbf{H}^i\right)^{-1}$, $\boldsymbol{\Delta} = \boldsymbol{\nabla}\mathcal{E}^{i+1} - \boldsymbol{\nabla}\mathcal{E}^i$, and

$$\mathbf{u} = \frac{\tilde{\boldsymbol{\delta}}^k}{(\tilde{\boldsymbol{\delta}}^k)^{\mathsf{T}}\cdot\boldsymbol{\Delta}} - \frac{\mathbf{C}^i\cdot\boldsymbol{\Delta}}{\boldsymbol{\Delta}^{\mathsf{T}}\cdot\mathbf{C}^i\cdot\boldsymbol{\Delta}}. \tag{6}$$

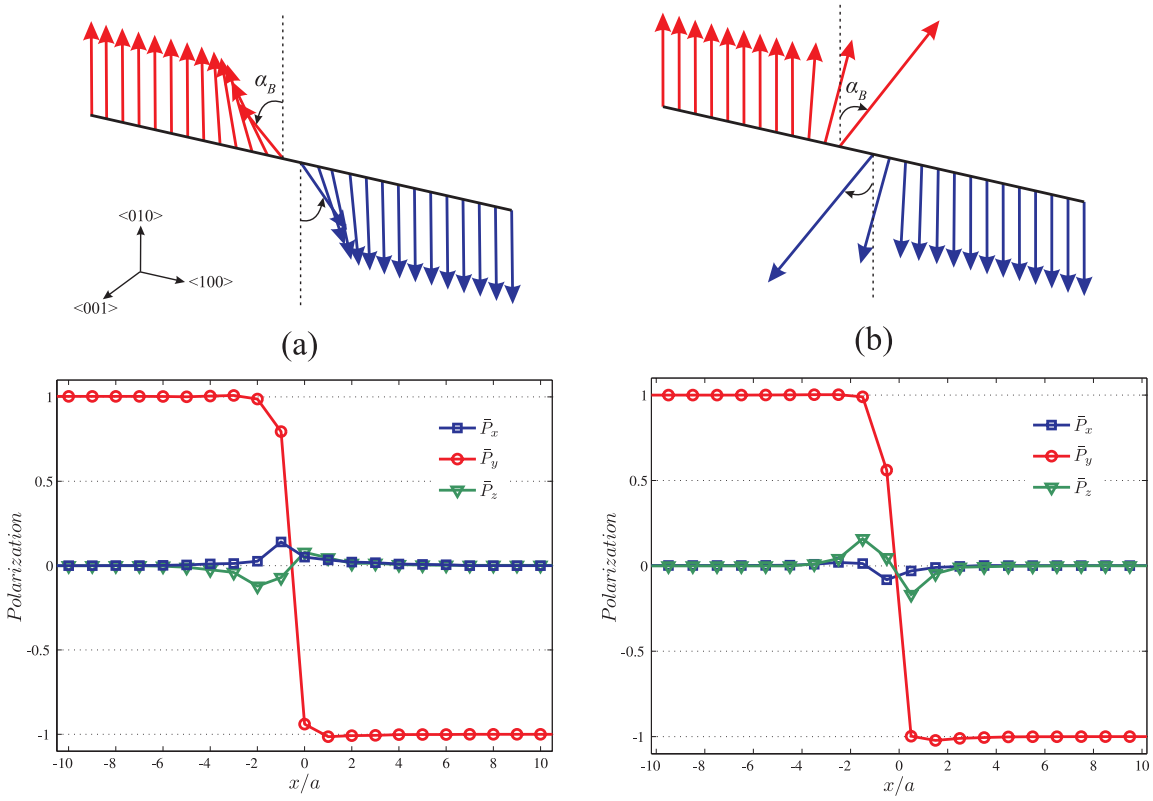

FIG. 4: The polarization vectors $\overline{\mathbf{P}} = (\bar{P}_x, \bar{P}_y, \bar{P}_z)$ for the row of unit cells on the section v-v with $d = a$ for: (a) Pb-Pb step and (b) Ti-Ti step. Close to the step, polarization rotates out of the (001)-plane with the Bloch angle α_B. The polarization also rotates inside the (001)-plane with the Néel angle α_N. Note that the Bloch and Néel components of the polarization correspond to the components in $\langle 001\rangle$-direction (P_z) and $\langle 100\rangle$-direction (P_x), respectively.

Calculating $\mathbf{C}^{i+1}$, one then should use $\mathbf{C}^{i+1}$ instead of $\mathbf{H}^{-1}$ to update the current configuration for the next configuration $\mathcal{B}^{k+1} = \mathcal{B}^k + \tilde{\boldsymbol{\delta}}^k$. If $\mathbf{C}^{i+1}$ is a poor approximation, then one may need to perform a linear search to refine $\mathcal{B}^{k+1}$ before starting the next iteration.

As the initial configuration for each step we start with two half lattices with the proper offset in the x-direction. The atomic configuration of each half lattice is the same as the atomic configuration in a perfect 180° domain wall. To remove the rigid body translation of the lattice, we fix the core of an atom in our computational box and fully relax the other atoms. Hence, we have $30W \times (L-3)$ variables in our calculations, where W and L are specified in Fig.2. To consider the effect of the atoms outside the computational box, we impose rigid body translations to these atoms as the boundary conditions, i.e., we rigidly move the atoms outside the computational box such that they keep the perfect 180° domain wall configuration. To this end, we rigidly move all of the atoms outside the computational box in the positive (negative) direction of the z-axis with the displacements equal to the displacement of the first (last) atom of the first (last) row of the representative layer of atoms. This is marked with the red (blue) circle in Fig.2(a). The displacements of the atoms outside the computational box in the positive (negative) direction of the x-axis are equal to the displacements of the atoms in the first (last) row of the computational box that is located on the same column. We choose $W = 20$ and $L = 30$ as we see larger values will not affect the results. In all our calculations we assume force tolerance of 0.05 eV/Å and observe that our solutions converge slowly after about 800 to 1000 iterations depending on the step type. Our calculations also show that using a smaller force tolerance of 0.005 eV/Å would change the results by less than 0.1%. This justifies the above choice of the force tolerance.

IV. NUMERICAL RESULTS

In this section we present our numerical results for the three different steps as follows. As we mentioned earlier, x, y, and z are coordinates along the $\langle 100\rangle$, $\langle 010\rangle$, and $\langle 001\rangle$-directions, respectively, and the origin of the coordinate system for each step is specified in Fig.2.

Pb-Pb step: The atomic configuration of Pb-cores in a Pb-Pb step are shown in Fig.3(a) and (b). For a clearer presentation of the atomic configuration, we have plotted the y-coordinates of Pb-cores for different sections v-v and h-h (see Fig.2). In Fig.3, s and d denote the distances of the h-h and v-v sections from the refer-

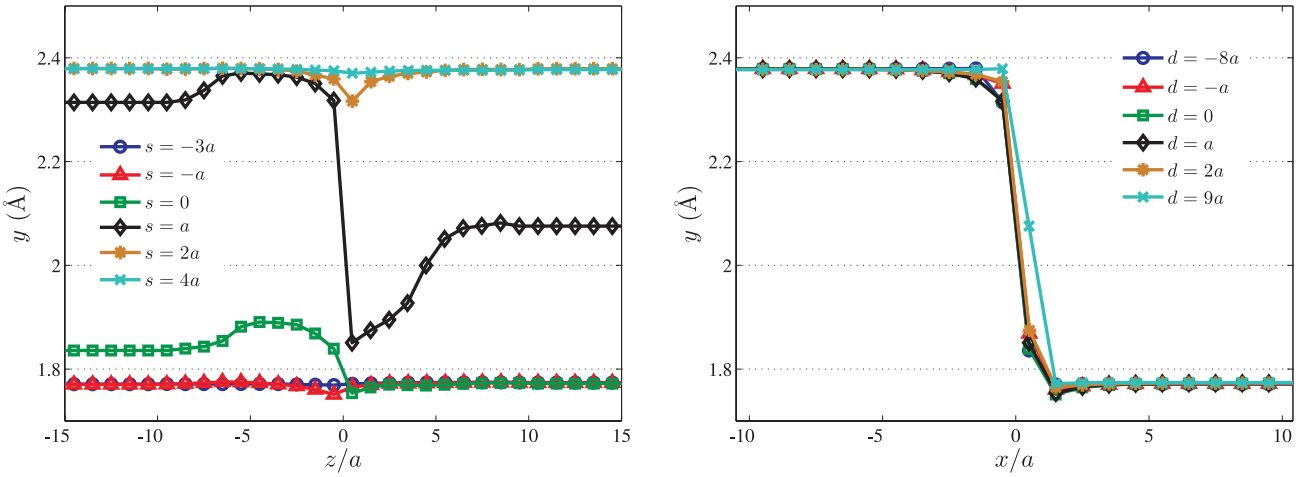

FIG. 5: The y-coordinates of Pb cores in a Pb-Ti step. Note that as it is shown in Fig.2, s and d denote the distances from the reference planes.

ence planes, respectively. Note that as is shown in Fig.2, the reference plane for v-v sections (r_v) is parallel to the (001)-plane and the reference plane for h-h sections (r_h) is parallel to the (100)-plane. As it can be seen, atomic distortions in the Pb-Pb step are localized, i.e, they are confined to a $8a \times 20a$ box in the (010)-plane. Atomic distortions in the $\langle 001 \rangle$-direction are less localized compared to those in the $\langle 100 \rangle$-direction. We observe that the step thickens the domain walls; the width of the domain wall near the step is about three times that of the prefect Pb-centered domain wall. Note that domain wall thickness cannot be defined uniquely very much like boundary layer thickness in fluid mechanics. Here, domain wall thickness is by definition the region that is affected by the domain wall, i.e. those layers of atoms that are distorted. One can use definitions like the 99%-thickness in fluid mechanics and define the domain wall thickness as the length of the region that has 99% of the far field rigid translation displacement. What is important here is that no matter what definition is chosen, domain wall "thickness" increases by the presence of steps. Note that due to the symmetry of the Pb-Pb step, atomic configuration for negative values of s and d will have the same behavior. Also note that the y-components of the atoms on the section $s = a$ in Fig.3(a) are not symmetric because of the way we define this section (see Fig.2). As the coordinates of cores and shells are close to each other, we only plot the results for cores. Also because other types of atoms display a similar behavior, we do not plot their coordinates here.

We follow Meyer and Vanderbilt [3] to calculate the polarization profile for each step. The polarization of unit cell i is calculated as

$$\mathbf{P}_i = \frac{e}{\Omega_c} \sum_j w_j Z_j^* \mathbf{u}_j^i, \qquad (7)$$

where e is the electron charge, Ω_c is the volume of the unit cell, Z_j^* is the Born effective charge tensor of the cubic $PbTiO_3$ bulk, and $\mathbf{u}_j^i$ denotes the displacement of the j-th atom of the unit cell i from the ideal lattice site. w_j denotes the weight for atom j. For example, for a Ti-centered unit cell we have $w_{Ti} = 1$, $w_O = 1/2$, and $w_{Pb} = 1/8$. We have plotted the polarization $\overline{\mathbf{P}}_i$ of the rows of unit cells on the section v-v with $d = a$ (see Fig.2) in a Pb-Pb step in Fig.4(a), where $\overline{\mathbf{P}}_i = \mathbf{P}_i/|\mathbf{P}_b|$, with $|\mathbf{P}_b|$ denoting the norm of the polarization of the bulk. We obtain the bulk polarization of 80.1 $\mu C\ cm^{-2}$, which is close to the published values 81.0 $\mu C\ cm^{-2}$ [22] and 81.2 $\mu C\ cm^{-2}$ [3]. We observe that near the step, the domain wall has a mixed Bloch-Néel character. Denoting the polarization components by $\overline{\mathbf{P}} = (\bar{P}_x, \bar{P}_y, \bar{P}_z)$, where $\bar{P}_x$, $\bar{P}_y$, and $\bar{P}_z$ are polarization components in $\langle 100 \rangle$, $\langle 010 \rangle$, and $\langle 001 \rangle$-directions, respectively, we observe that the polarization vector rotates out of the (001)-plane with the Bloch angle $\alpha_B = \tan^{-1}\left(\bar{P}_z/\bar{P}_y\right)$ (see Fig.4). The maximum rotation angle α_B for Pb-centered domain wall is $\alpha_B \simeq 7.0°$. Also the polarization rotates in the (001)-plane with the Néel angle $\alpha_N = \tan^{-1}\left(\bar{P}_x/\bar{P}_y\right)$. The maximum value of α_N for Pb-centered wall is $\alpha_N \simeq 9.9°$ (compare this with $\alpha_N = 1.43°$ for the perfect domain wall [13]). The maximum value of the polarization in the $\langle 100 \rangle$ and $\langle 001 \rangle$-directions are about 13.9% and 12.2% of the bulk polarization, respectively.

Finally, we calculate the energy of the Pb-Pb step, E_{Pb-Pb}. Similar to the domain wall energy, we define the step energy to be the difference in energies of the unit cells inside the computational box that are located on the domain wall with the step and bulk energy of the same number of unit cells, divided by the total area of domain wall in the system. This way we obtain the Pb-Pb step energy to be 157 mJm^{-2}, which is greater than the Pb-centered domain wall energy that is 132 mJm^{-2} [3].

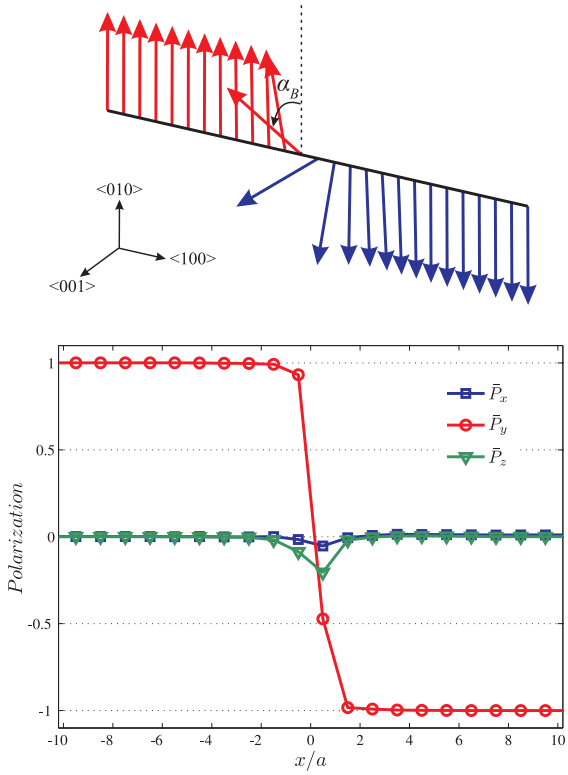

FIG. 6: The polarization vectors $\overline{\mathbf{P}} = (\bar{P}_x, \bar{P}_y, \bar{P}_z)$ for the row of unit cells on the section v-v with $d = a$ for a Pb-Ti step. Close to the step, polarization rotates out of the (001)-plane with the Bloch angle α_B. The polarization also rotates inside the (001)-plane with the Néel angle α_N. Note that the Bloch and Néel components of the polarization correspond to the components in $\langle 001 \rangle$-direction (P_z) and $\langle 100 \rangle$-direction (P_x), respectively.

Ti-Ti step: Figs.3(c) and (d) depict the y-coordinates of Ti cores in a Ti-Ti step for different sections v-v and h-h. Again because of symmetry, we plot the results only for positive values of s and d and also similar to the Pb-Pb step, by definition of the section $s = a$, the y-components of the atoms on this section in Fig.3(c) are not symmetric. Similar to the Pb-Pb step, we observe that the Ti-Ti step is localized, i.e., atomic distortions are confined to a $9a \times 18a$ box in the (010)-plane. Again we observe that the step thickens the Ti-centered domain wall; the thickness of the defective wall is about three times that of the perfect domain wall.

As is shown in Fig.4(b), polarization has a mixed Bloch-Néel character near the step. For the Ti-Ti step, the maximum value of the Bloch and Néel rotation angles are $\alpha_B \simeq 9.5°$ and $\alpha_N \simeq 8.1°$ (compare this with $\alpha_N = 1.0°$ in the perfect domain wall [13]), respectively. The maximum value of the polarization in the $\langle 100 \rangle$ and $\langle 001 \rangle$-directions are about 8.1% and 16.8% of the bulk polarization, respectively. The energy of the Ti-Ti step is $E_{Ti-Ti} = 172\ mJm^{-2}$, which is larger than the energy of the Pb-Pb step and the energy of the Ti-centered domain wall, which is 169 mJm^{-2} [3]. This is consistent with the fact that Ti-centered 180° domain walls have a greater static energy than Pb-centered domain walls [3, 6].

Pb-Ti step: We have plotted the y-coordinates of Pb cores in a Pb-Ti step in Fig.5 for different v-v and h-h sections. Note that because Pb-Ti steps are not symmetric, we have plotted the results for both positive and negative values of s and d. Also since other types of cores and shells have a similar behavior, we do not plot their coordinates here. We observe that similar to the other two steps, the Pb-Ti step causes local distortions that are confined to a $6a \times 16a$ box in (010)-plane. The step broadens the domain wall; the defective domain wall thickness is twice that of the perfect domain wall. Note that the Pb-centered and Ti-centered domain walls for this step are half a lattice spacing apart and this may explain the weaker thickening effect of the Pb-Ti step.

As Fig.6 shows polarization distribution has a mixed Bloch-Néel character near the Pb-Ti step but the Bloch character is more dominant. The Polarization profile is plotted for the row of unit cells on the section v-v with $d = a$, which is located in the Ti-centered part of the step. For the Pb-Ti step, the maximum value of the Bloch and Néel rotations are $\alpha_B \simeq 23.0°$ and $\alpha_N \simeq 5.9°$, respectively. The maximum value of the polarization in the $\langle 100 \rangle$ and $\langle 001 \rangle$-directions are about 5.3% and 20.5% of the bulk polarization, respectively. The energy of the Pb-Ti step is $E_{Pb-Ti} = 165\ mJm^{-2}$. It is seen that $E_{Pb-Pb} < E_{Pb-Ti} < E_{Ti-Ti}$.

V. CONCLUDING REMARKS

In this work we obtained the atomic structure of three different types of steps on 180° domain walls in $PbTiO_3$ using the method of anharmonic lattice statics. We observe that these steps cause local atomic distortions that are confined to a box with dimensions of a few lattice spacings. All the three steps have a broadening effect on the domain wall thickness. Pb-Ti steps have a less broadening effect compared to the other two steps.

We also observe that steps on 180° domain walls can cause the polarization profile to have a mixed Bloch-Néel character. The Bloch character is more dominant in Ti-Ti and Pb-Ti steps. Finally, we observe that the Pb-Pb step has a lower static energy than the other two steps.

Acknowledgments

Study of steps on ferroelectric domain walls was suggested to the second author by Professors Michael Ortiz and Kaushik Bhattacharya. We thank an anonymous referee for useful comments that improved the presentation of our work.

[1] S. V. Kalinin, A. N. Morozovska, L. Q. Chen and B. J. Rodriguez, *Rep. Prog. Phys.*, **73** , 056502 (2010).

[2] M. Dawber, K. M. Rabe and J. F. Scott, *Rev. of Modern Phys.*, **77** , 1083 (2005).

[3] B. Meyer and D. Vanderbilt *Phys. Rev. B*, **65**, 1 (2001).

[4] J. Padilla, W. Zhong and D. Vanderbilt *Phys. Rev. B*, **53**, R5969 (1996).

[5] A. Yavari, M. Ortiz and K. Bhattacharya, *Philos. Mag.*, **87** , 3997 (2007).

[6] A. Angoshtari and A. Yavari, *EPL*, **90**, 27007 (2010).

[7] J. Hlinka and P. Marton, *Phys. Rev. B*, **74**, 104104 (2006).

[8] M. Iwata, K. Katsuraya, I. Suzuki, M. Maeda, N. Yasuda and Y. K. Ishibashi, *Jpn. J. Appl. Phys.*, **42**, 6201 (2003).

[9] P. Lehnen, J. Dec and W. Kleemann, *J. Phys. D: Appl. Phys.*, **33**, 1932 (2000).

[10] D. Shilo, G. Ravichandran and K. Bhattacharya, *Nature Mater.*, **3**, 453 (2004).

[11] W. T. Lee, E. K. H. Salje and U. Bismayer, *Phys. Rev. B*, **72**, 104116 (2005).

[12] A. Angoshtari and A. Yavari, *Comput. Mater. Sci.*, **48**, 258 (2010).

[13] D. Lee, R. K. Behera, P. Wu, H. Xu, Y. L. Li, S. B. Sinnott, S. R. Phillpot, L. Q. Chen and V. Gopalan, *Phys. Rev. B*, **80**, 060102(R) (2009).

[14] I. I. Naumov, L. Bellaiche and H. X. Fu, *Nature*, **432**, 737 (2004).

[15] S. Prosandeev, I. Ponomareva, I. Naumov, I. Kornev and L. Bellaiche, *J. Phys.: Condens. Matter*, **20**, 193201 (2008).

[16] R. E. Nettleton, *J. Phys. Soc. Jpn.*, **22**, 1375 (1967).

[17] V. Y. Shur, A. L. Gruverman and E. L. Rumyantsev, *Ferroelec.*, **111**, 123 (1990).

[18] Y. H. Shin, I. Grinberg, I. W. Chen and A. M. Rappe, *Nature*, **449**, 881 (2007).

[19] A. Yavari, M. Ortiz and K. Bhattacharya, *J. Elasticity*, **86**, 41 (2007).

[20] A. Yavari and A. Angoshtari, *Inter. J. Solids Struct.*, **47**, 1807 (2010).

[21] A. Asthagiri, Z. Wu, N. Choudhury and R. E. Cohen, *Ferroelec.*, **333** , 69 (2006).

[22] R. K. Behera, B. B. Hinojosa, S. B. Sinnott, A. Asthagiri S. R. Phillpot, *J. Phys.: Condens. Matter*, **20**, 395004 (2008).

[23] D. P. Wolf, P. Keblinski, S. R. Phillpot and J. Eggebrecht, *J. Chem. Phys.*, **110**, 8254 (1999).

[24] W. H. Press, S. A. Teukolsky, W. T. Vetterling, and B. P. Flannery, *Numerical recipes: the art of scientific computing* (Cambridge University Press, Cambridge, 1989).

[25] We assume that this offset is one or half a lattice spacing.